Compact wavelength blocker based on silicon microring resonator with nested pair of subrings

Jiayang Wu, Ting Pan, Pan Cao, Xiaofeng Hu, Lipeng Jiang, Xinhong Jiang, and Yikai Su
State Key Laboratory of Advanced Optical Communication Systems and Networks, Department of Electronic Engineering, Shanghai Jiao Tong University, Shanghai 200240, China

Paper Summary
We propose and experimentally demonstrate a compact wavelength blocker implemented by silicon micoring resonator (MRR) with nested pair of subrings, which can perform selective channel-blocking at certain resonances of the MRR without affecting the others.

Introduction

Ever-increasing network capacity and efficiency are driving the demand for high-performance channel management technologies in wavelength division multiplexing (WDM) optical communication networks. Reconfigurable optical add-drop multiplexers (ROADMs), which enable flexible and efficient management of wavlength channels, are key building blocks for the next-generation WDM networks [1-2]. Wavelength blockers are core components in most ROADM systems [3-5]. By controlling the attenuation of each individual channel, wavelength blockers can perform selective channel-blocking and dynamic channel equalization.

Various schemes have been proposed to implement wavelength blockers based on microelectromechanical systems (MEMS) [6-7], liquid crystal (LC) [8-9], and planar lightwave circuits (PLCs) [10-11]. Amongst them, the wavelength blockers based on PLCs can offer advantages of compactness, improved stability, and capability of large-scale integration. Since silicon microring resonators (MRRs) are integrated comb filters widely employed in optical networks-on-chip (NoC) [12], it would be desired to implement an integrated wavelength-blocker by selectively blocking certian resonances of a MRR. However, it has been proved to be difficult to control certain resonances of a single MRR without affecting the others [13].

In this paper, we propose and experimentally demonstrate an on-chip wavlength blocker implemented by a silicon MRR with nested pair of subrings (MRR-NPS). Owing to resonance splitting induced by the inner NPS, the proposed device is capable of blocking certian resonances of the outer MRR. System demonstration of selective channel-blocking with 10-Gb/s NRZ signal is performed. The expeimental results further verify the effectiveness of the fabricated device as an on-chip wavelength blocker.

Device configuration and operation principle

Fig. 1(a) illustrates the schematic diagram of the proposed MRR-NPS. There is a pair of mutually coupled

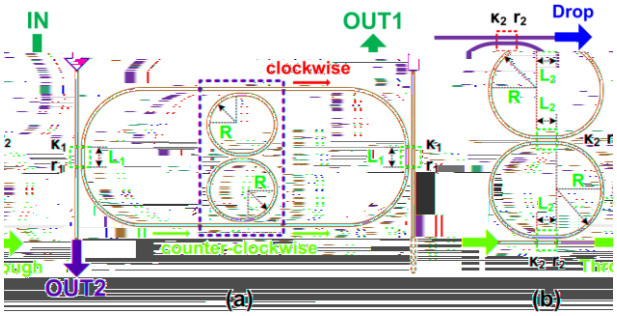

Fig. 1. (a) Schematic diagram of the proposed MRR-NPS. (b) Zoom-in view of the NPS marked with dashed box in (a).

subrings nested inside the outer MRR, which excites a mode circulating in a direction opposite to that of the mode in the outer MRR. As a result of the coherent interference between the two degenrated modes circulating in opposite directions [14], there are split resonances in the transmission spectra from IN to OUT1 and from IN to OUT2, as shown in Fig. 2(a) and (b), respectively. The transmission spectra are calculated by using the scattering matrix method (SMM) [15]. The transfer function from IN to OUT1 can be expressed as:

$$T_{out1} = \frac{-\sqrt{A}\kappa_1^2\, e^{i\Phi/2} M_T[1 - Ar_1^2\, e^{i\Phi}(M_T^2 - M_D^2)]}{1 - 2Ar_1^2\, e^{i\Phi} + A^2 r_1^4\, e^{2i\Phi}(M_T^2 - M_D^2)^2}, \quad (1)$$

where M_T and M_D denote the transfer functions for the through and drop ports of the NPS shown in Fig. 1(b), respectively, which can be given by:

$$M_T = \frac{r_2[1-(r_2^2+1)a\, e^{i\varphi} + a^2\, e^{2i\varphi}]}{1 - 2ar_2^2\, e^{i\varphi} + a^2 r_2^2\, e^{2i\varphi}},$$
$$M_D = \frac{-ia\kappa_2^3\, e^{i\varphi}}{1 - 2ar_2^2\, e^{i\varphi} + a^2 r_2^2\, e^{2i\varphi}}. \quad (2)$$

In Eq. (1) and (2), r_i and κ_i (i = 1, 2) are the transmission and coupling coefficients of the two kinds of directional couplers shown in Fig. 1(a) and (b), respectively. A and a are the tranmission factors along the outer ring and one of the inner subrings, respectively. Φ and φ are the phase

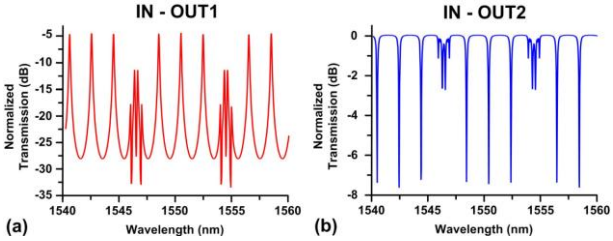

Fig. 2. (a) Normalized transmission spectrum from IN to OUT1. (b) Normalized transmission spectrum from IN to OUT2.

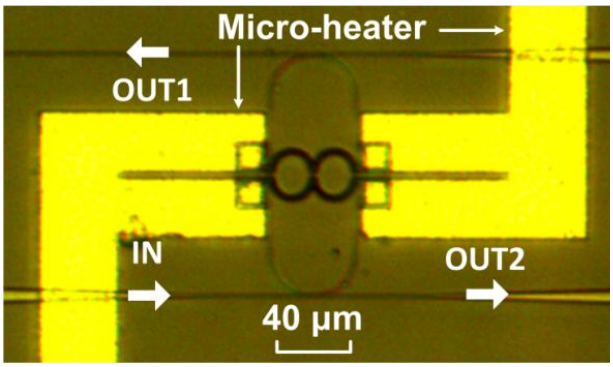

Fig. 3. Micrograph of the fabricated device.

shifts along the outer ring and one of the inner subrings, respectively.

The structural parameters are chosen as follows: the gap size in the coupling region is 0.18 μm, and the coupling lengths are $L_1 = L_2 = 3$ μm. The radius of each subring is $R = 10$ μm, and the circumference of the outer microring is four times as large as that of each subring. For silicon photonic waveguides with a cross section of 450×220 nm^2 designed to be single mode at 1550 nm, the transmission coefficients of the directional couplers calculated by using Lumerical finite-difference time-domain (FDTD) Solutions are $r_1 = r_2 = 0.9506$. Based on our previously fabricated devices, the waveguide group index of the transverse electric (TE) mode and the waveguide loss factor are assumed to be $n_g = 4.3350$ and $\alpha = 460$ m^{-1}, respectively. In Fig. 2(a), one can see that there is a split resonance in any four adjacent resonances of the outer MRR. The transmissions at the central wavelengths of the split resonances are ~23 dB lower than those of the unsplit resonances, which can be used to block certain resonance wavelengths of the outer MRR without affecting the others. An increased ratio between the circumference of the outer ring and the inner subring would result in increased number of unsplit resonances between the adjacent split resonances.

Device fabrication and measured spectra

The proposed device based on the above design parameters is fabricated on an 8-inch silicon-on-insulator (SOI) wafer with a 220-nm-thick top silicon layer and a 2-μm-thick buried dioxide (BOX) layer. The entire fabrication process is CMOS compatible, with no further requirement for high-temperature post-processing. The micrograph of the fabricated device is shown in Fig. 3. 248-nm deep ultraviolet (DUV) photolithography is utilized to define the layout, and an inductively coupled plasma (ICP) etching process is used to etch the top silicon layer. Thermal-optic micro-heater is fabricated along the NPS to tune the central wavelengths of the split resonances. Grating coupler for TE polarization is employed at each end to couple light into/out of the device with single-mode fibers.

The normalized transmission spectrum from IN to OUT1 measured with the fabricated device is shown in

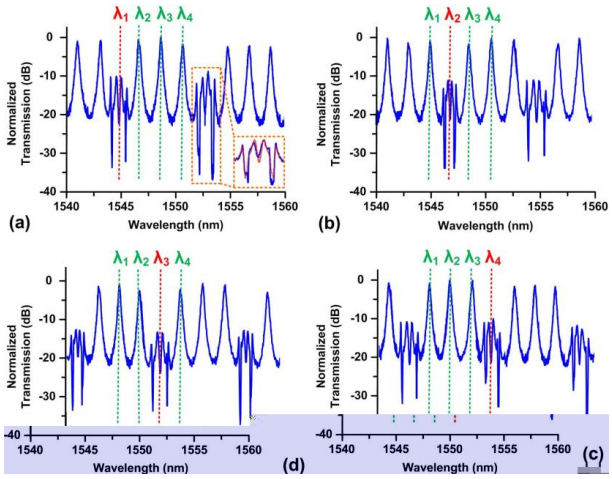

Fig. 4. (a) Measured transmission spectrum from IN to OUT1. Inset shows zoom-in spectrum around one split resonance fitted by the red dashed curve calculated from Eq. (1) and (2). (b) ~ (d) Measured transmission spectra from IN to OUT1 when the DC voltages applied to the micro-heater are 0.4 V, 0.7 V, and 1.0 V, respectively.

Fig. 4(a) by the blue solid curve. The on-chip insertion loss is ~10.2 dB. The zoom-in spectrum around one of the split resonances is fitted by the red dashed curve calculated from Eq. (1) and (2), as shown in the inset of Fig. 4(a). It can be seen that the measured curve fits well with the calculated one. The fitting parameters are $r_1 = r_2 \approx 0.9498$, $\alpha \approx 502$ m^{-1}, and $n_g \approx 4.3312$, which are consistent with our expectations before fabrication. In Fig. 4(a), λ_1, λ_2, λ_3, and λ_4 denote the central wavelengths of four adjacent resonances of the outer MRR. The resonance at $\lambda_1 = 1544.812$ nm is split, whereas the resonances at $\lambda_2 = 1546.810$ nm, $\lambda_3 = 1548.808$ nm, and $\lambda_4 = 1550.806$ nm are not. The transmission at λ_1 is ~20 dB lower than those at λ_2, λ_3, and λ_4, meaning that the central wavelength of the split resonance is blocked by the MRR-NPS with an exrinction ratio of ~20 dB.

By applying a DC voltage to the thermal-optic micro-heater along the NPS, the cental wavelengths of the split resonances are redshifted. When the DC voltages applied to the micro-heater are 0.4 V, 0.7 V, and 1.0 V, the measured transmission spectra from IN to OUT1 are shown in Fig. 4(b), (c), and (d), respectively. The resonances at λ_2, λ_3, and λ_4 are split in Fig. 4(b), (c), and (d), respectively, thus leading to selective wavelength-blocking at λ_2, λ_3, and λ_4 accordingly. It should be noted that during the thermal-optic tuning process, the resonance wavelengths of the outer MRR are almost fixed, since the DC voltages applying on the micro-heater along NPS do not shift the resonance wavelengths of the outer MRR.

System demonstration of channel-blocking

We use the experimental setup shown in Fig. 5 to test the performance of the fabricated device as a wavelength blocker. The continuous-wave (CW) light lauched by a tunbale laser is modulated by a Mach–Zehnder

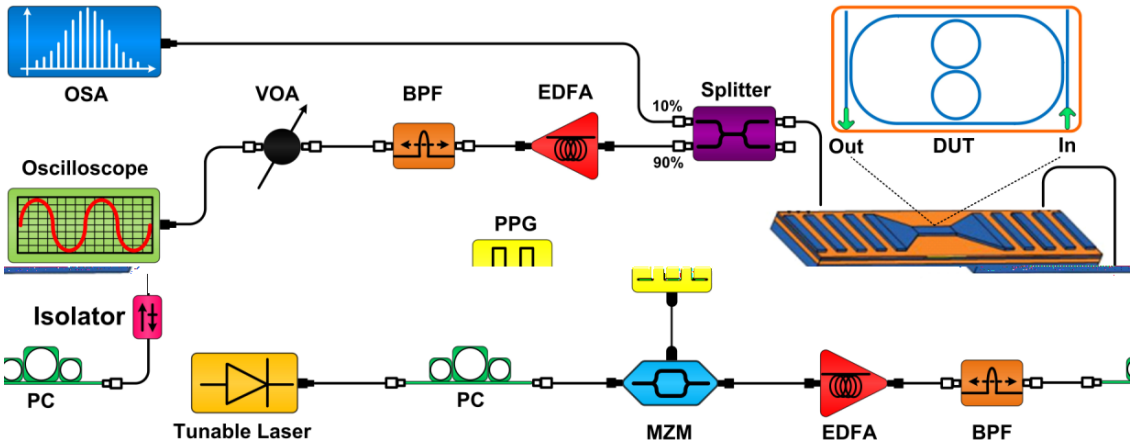

Fig. 5. Experimental setup for system demonstration of selective channel-blocking using the fabricated device. PC: polarization controller, MZM: Mach–Zehnder modulator, PPG: pulse pattern generator, EDFA: erbium-doped fiber amplifier, BPF: band-pass filter, DUT: device under test, VOA: variable optical attenuator, OSA: optical spectrum analyzer.

modulator (MZM) driven by a 10-Gb/s electrical pseudo random bit sequence (PRBS) signal from a pulse pattern generator (PPG). The MZM is biased at quadrature point of the transmission curve to generate non-return-to-zero (NRZ) signal. The generated NRZ signal is amplified by an erbium-doped fiber amplifier (EDFA) followed by a tunable band-pass filter (BPF) to suppress the amplified spontaneous emission (ASE) noise. A polarization controller (PC) is inserted before the device under test (DUT) to make sure that the input signal is TE polarized, followed by an isolator to block the reflection of the undesired modes. Vertical coupling system is employed to couple light into and out of the DUT. The output signal after going through the DUT is split into two parts by using a 90:10 fiber splitter. One part is fed into an optical spectrum analyzer (OSA), and the other goes to an oscilloscope after being amplified by another EDFA with one more BPF to suppress the ASE noise.

When the wavelength of the CW light is set to λ_1, λ_2, λ_3, and λ_4 in Fig. 5 (a), respectively, the eye diagrams of the output signals recorded by the oscilloscope are shown in Fig. 6(a) accordingly. The input NRZ signal is blocked at λ_1 as a result of resonance splitting, and one can not observe the opened eye diagram at this wavelength. When the DC voltages applied to the micro-heater are 0.4 V, 0.7 V, and 1.0 V, the input signals are blocked at λ_2, λ_3, and λ_4 with closed eye diagrams, as shown in Fig. 6(b), (c), and (d), respectively.

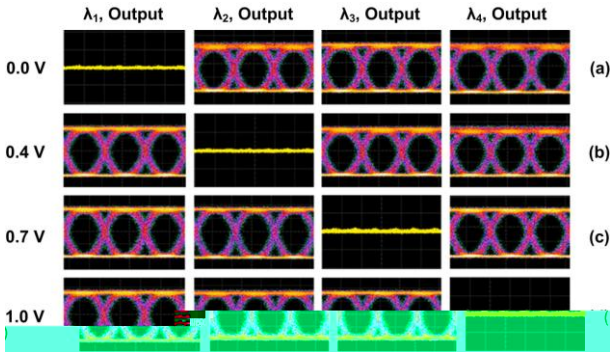

Fig. 6. (a) ~ (d) Eye diagrams of 10-Gb/s output NRZ signals at wavelengths of $\lambda_1 \sim \lambda_4$ when the DC voltages applied to the micro-heater are 0.0 V, 0.4 V, 0.7 V, and 1.0 V, respectively.

Conclusions

In conclusion, we have proposed and experimentally demonstrated a on-chip wavelength blocker based on silicon MRR-NPS. The proposed device can be used to selectively block certian resonances of the MRR without affecting the others. The peformance of the fabricated device as an effective wavelength blocker is tested by the system experiment with 10-Gb/s NRZ signal.

Acknowledgement

This work was supported in part by NSFC (61125504/61235007), MoE (20110073110012), and Minhang Talent Program. We also acknowledge IME Singapore for device fabrication.

References

1. T. Strasser, et al, J. Sel. Top. Quantum. Electron., 16 (2010) p. 1150.
2. N. Kataoka, et al, J. Lightw. Technol., 24 (2006), p. 88.
3. J. Rhee, et al, J. Lightw. Technol., 21 (2003), p. 25.
4. E. Basch, et al, J. Sel. Top. Quantum. Electron., 12 (2006) p. 615.
5. R. Shankar, et al, Opt. Commun., 279 (2007), p. 94
6. J. Ford, et al, J. Lightw. Technol., 17 (1999), p. 904.
7. D. Marom, et al, J. Lightw. Technol., 23 (2005), p. 1620.
8. J. Ertel, et al, J. Lightw. Technol., 24 (2006), p. 1674.
9. E. Nicolescu, et al, J. Lightw. Technol., 28 (2010), p. 3121.
10. Y. Goebuchi, et al, Photon. Technol. Lett., 18 (2006), p. 538.
11. W. Bogaerts, et al, J. Sel. Top. Quantum. Electron., 12 (2006) p. 1394.
12. S. Feng, et al, Laser Photonic Rev., 6 (2012) p. 145.
13. Y. Wen, et al, Phys. Rev. Lett., 108 (2012) p. 223907.
14. Q. Li, et al, Opt. Exp. 17(2009) p. 933.
15. J. Wu, et al, Photon. Technol. Lett. 25 (2013) p.580.